PNAS

Supporting Information for

Identification of broad, potent antibodies to functionally constrained regions of SARS-CoV-2 Spike as part of a polyclonal response to a breakthrough infection

Jamie Guenthoer[1], Michelle Lilly[1], Tyler N. Starr[2], Bernadeta Dadonaite[3], Klaus N. Lovendahl[4], Jacob T. Croft[4], Caitlin I. Stoddard[1], Vrasha Chohan[1], Shilei Ding[5], Felicitas Ruiz[1], Mackenzie S. Kopp[1], Andrés Finzi[5,6], Jesse D. Bloom[3,7,8], Helen Y. Chu[9], Kelly K. Lee[4], Julie Overbaugh[1,7]*

Corresponding Author:
Julie Overbaugh
Email: joverbau@fredhutch.org

This PDF file includes:

Supplemental Methods

Memory B cell sort and reconstruction of antibodies

Thirty-day post symptom onset PBMCs were stained using a mouse anti-human antibody cocktail to cell surface markers: CD3-BV711 (BD Biosciences, clone UCHT1), CD14-BV711 (BD Biosciences, clone MφP9), CD16-BV711 (BD Biosciences, clone 3G8), CD19-BV510 (BD Biosciences, clone SJ25C1), IgM-FITC (BD Biosciences, clone G20-127), IgD-FITC (BD Biosciences, clone IA6-2) to allow for identification of memory B cells. Spike-specific B cells were isolated by incubating with a pool of APC/PE-labeled Delta HexaPro spike protein and spike S2 peptide (Acro Biosystems, cat. S2N-C52E8). The B cells that bound to the spike baits were single-cell sorted on a BD FACSAria II into 96-well plates containing cell lysis/RNA storage buffer and immediately snap-frozen and stored at -80°C. Three hundred and eighty-four single B cells were collected in this sort.

Antibody gene sequences were recovered from the sorted B cells using established methods (1, 2) starting with one 96-well plate of the collected B cells. In brief, total RNA from each sorted cell was reverse transcribed using Superscript III (Invitrogen) and random primers (Invitrogen). Then, the IgG heavy (Igγ) and light chain variable regions (Igκ, Igλ) were amplified using semi-nested PCRs with previously described primer sets (3, 4). Products were sequenced, aligned with Geneious (v10.0.8, Dotmatics), and analyzed for consensus with functional heavy and light chain variable regions sequences using the IMGT V-QUEST tool to identify “productive sequences" (5). Productive sequences are designated by the IMGT V-QUEST tool as being a recognized, rearranged Igγ, Igκ, or Igλ sequence that is in frame with no stop codon. The productive sequences we identify with a paired heavy and light chain were cloned into Igγ1, Igκ, and/or Igλ expression vectors as previously described (1, 2, 6). Monoclonal antibodies were produced using standard methods in FreeStyle™ 293-F Cells (Invitrogen) (2, 7, 8).

Variable region protein sequences for C68.3, C68.13, C68.59 C68.61 mAbs

C68.3_IgH
QVQLVESGPGLVKPSETLSLTCTVSGASISTSSDYWGWIRQPPGKGLEWIGSTHYSGSTHYNPSLKSRVTISV
DTSKNQFSLKLSSVTAADTAVYYCARGFEPEYWGQGTLVTVSS

C68.3_IgL
SYELTQSPSVSVAPGKTARITCGGNNIGSKSVHWYQQKPGQAPVLVVYNDSDRPSGIPERFSGSNSGNTATLT
ISRVEAGDEADYYCQVWDSTSDHPRVVFGGGTKLTVP

C68.13_IgH
QVQLVESGGGVVQPGRSLRLSCAASGFTFSTYAMHWVRQAPGKGLEWVAVISFDGSNTYYADSVKGRFTISR
DNSKNTLYLQMNSLRAEDTAVYYCAKDSYYSDRSDYYWRSYGYFDLWGQGTLVTVSS

C68.13_IgK
DIQLTQSPSTLSASVGDRVTITCRASQSISSWLAWYQQKPGKAPKLLIYDASSLESGVPSRFSGSGSGTEFTLTI
SSLQPDDLATYYCQQYRSYSGTFGQGTKVEIK

C68.59_IgH
EVQLVESGGGLIQPGGSLRLSCAASGLTFTNYWMLWVRQAPGKGLVWVSHINSDGSSTNNADSVKGRFTISR
DNAKNTLYLQMNSLRDEDTAVYYCGGTYCTGGSCGIVYWGQGTLVTVSS

C68.59_IgL
SYELTQPPSVSVSPGQTASITCSGDKLGDKYVFWYQQKSGQSPALVIYQDSLRPSGIPDRFSGSNAGNTATLTI
SGTPAVDEADYYCQAWDSSTLVFGGGTKLTVL

C68.61_IgH
EVQLVQSGAEVKKPGESLKISCKGSAYIFTRYWIGWVRQMPGKGLEWMGIIYPGDSDTRYSPSFQGQVTISAD
KSISTAYLQWSSLKASDTAMYYCARSGTTNYFDYWGQGTLVTVSS

C68.61_IgK
DIQLTQSPSTLSASVGDRVTITCRASQSISSWLAWYQQKPGKAPKLLIYDASSLDSGVPSRFSGSGSGTDFTLTI
SSLQPDDFATYYCQQFNSYWTFGQGTKVEIK

Binding and epitope mapping by Direct and Competition ELISAs

The binding affinities of the mAbs to recombinant stabilized spike trimers were assessed by direct ELISA as previously described (9, 10). The recombinant spike trimers used in these assays were as follows: Wuhan-Hu-1 (Sino Biologics, cat. 40589-V08H4), Delta (Sino Biologics, cat. 40589-V08H10), Omicron BA.1 (Sino Biologics, cat. 40589-V08H26), Omicron BA.2 (Sino Biologics, cat. 40589-V08H28), Omicron BA.4/BA.5 (Sino Biologics, cat. 40589-V08H32), Omicron XBB (Sino Biologics, cat. 40589-V08H40), Omicron BQ.1.1 (Sino Biologics, cat. 40589-V08H41), and SARS-CoV-1 (Acro Biosystems). The spike subdomain peptides were RBD (cat. 40592-V08B), NTD (cat. 40591-V49H), S2 (cat. 40590-V08B); Sino Biologics). Recombinant protein was coated onto 384-well ELISA plates at 1 μg/mL overnight at 4°C. The plate was washed 4x with wash buffer (PBS with 0.01% Tween-20) and blocked with 3% nonfat dry milk in wash buffer for one hour at room temperature. Each mAb was normalized to 1 μg/mL and serially diluted 2-fold for 13 total dilutions and added to the plate in technical replicates. The influenza-specific antibody FI6V3 or HIV-specific mAb VRC01 were included as a

negative control. Plates were incubated for 1 hour at 37°C and samples were washed 4x. Secondary antibody, goat anti-human IgG-Fc HRP-conjugated antibody, was applied and incubated for 1 hour at room temperature, followed by four additional washes. TMB substrate was added and following a four-to-six minute incubation, the reaction was stopped with 1N sulfuric acid. The absorbance at OD450 nm was read. For the spike subunit ELISAs (NTD, RBD and S2), C68.59 mAb was diluted to 50 μg/mL, 25 μg/mL, 12.5 μg/mL, and 2 μg/mL to assess binding at higher concentrations. mAbs with known spike epitopes were included as positive controls and diluted to 2 μg/mL: LY-CoV555 (RBD-specific), CV3-25 (S2-specific)(11), CV3-13 (NTD-specific)(12). The EC50s were calculated with a non-linear regression fit for agonist versus response after background correcting with the negative control wells and constraining the maximal absorbance value to the average maximum absorbance of a positive control mAb (LY-CoV1404 for the SARS-CoV-2 VOCs, S309 for SARS-CoV-1, LY-CoV555 for RBD).

Competition ELISAs to map epitopes of RBD-specific mAbs or determine ACE2-binding interference were performed as previously described, with some modifications (13). The RBD-specific mAbs used in the competition ELISAs including the following: LY-CoV016/etesevimab (InvivoGen, cat. srbdc6-mab1); LY-CoV555/bamlanivimab (InvivoGen, cat. srbdc5-mab1); REGN10987/imdevimab (InvivoGen, cat. srbdc4-mab1); CR3022 (Abcam, cat. ab273073); 309/sotrovimab precursor (BioVision, cat. A2266). LY-CoV-1404/bebtelovimab antibody variable domain sequences were acquired from the structure reported in (14) and recombinant antibody was cloned and produced by GenScript. mAbs or ACE2 protein were first biotinylated using the EZ-Link Sulfo-NHS-Biotinylation Kit (Thermo Fisher Scientific) followed by removal of unreacted biotinylation reagents using a Zeba Spin Desalting Column (Thermo Fisher Scientific) per the manufacturer's recommended protocols. Plates were coated with prefusion stabilized Wuhan-Hu-1 6P spike (Sino Biologics, cat. 40589-V08H4) at 1 μg/mL in 1X PBS overnight at 4°C and blocked with 3% BSA in wash buffer for one hour at 37°C. Plates were washed as described above. A four-fold dilution series was generated with the non-biotinylated ("blocking") mAb in wash buffer starting at 10 μg/mL. After the block was removed, the dilution series was applied to the plate and incubated for 15 min at 37°C. The plate was washed, and the biotinylated

("competing") protein was added at 0.1 μg/mL followed by incubation at 37°C for 45 minutes. The remaining steps were completed as described above. The absorbance at OD450 nm was read. Each combination of blocking-competing mAbs was reversed to confirm competition. Each mAb was also competed against itself. The HIV-specific mAb VRC01 was included as a negative control on all plates. Data were analyzed and plotted using GraphPad Prism (v9). For the mAb/mAb competition ELISAs, background signal from negative control wells was subtracted, and the % competition was calculated as 100*((1/Y)/(1/K)) where Y was the area under the curve (AUC) from the dilution series of the blocking antibody of interest and K was the AUC of the self-competition condition. For the ACE2-binding inhibition ELISAs, the background signal from the average of the negative control wells was subtracted from each well and the AUCs from the dilution series of each mAb and the negative control were calculated. The % inhibition was calculated as 100 * (1 - (mAb $AUC_{corrected}$/NegContol $AUC_{corrected}$)).

Spike-pseudotyped lentivirus neutralization assay

Spike-pseudotyped lentiviruses were produced and their infectious titers determined as previously described (10, 15). Codon-optimized plasmids with spike genes specific for WH-1, Delta, Omicron BA.1, Omicron BA.2, Omicron BA.4/BA.5, Omicron BA.2.12.1, SARS-CoV-1 were obtained (WH-1, BA.1, BA.2 were produced in the Bloom lab; Delta was a gift from Amit Sharma, BA.4/5, BA2.12.1, XBB, XBB.1.5, XBB.4, BQ.1.1, and SARS-CoV-1 gifts from Marceline Côté). Vectors with the spike genes from one of the SARS-CoV-2 VOCs or SARS-CoV-1 were co-transfected with lentiviral helper plasmids into HEK293T cells. At 50-60 hours post transfection, the supernatant containing virus was collected, filtered, and concentrated. The viral titer was determined by infecting HEK293T-ACE2 cells and measuring relative luciferase units (RLUs). The HEK293T-ACE2 cells used express high levels of ACE2 as described previously (15, 16).

Neutralization of the pseudoviruses by the plasma and mAbs was performed as previously described (9, 15). HEK293T-ACE2 cells were seeded at ~4000 cells/well in DMEM (supplemented with 10% FBS and penicillin/streptomycin/fungizone) in a black-walled 384 well plate. HEK293T cells were also plated in separate wells as controls. A two or three-fold serial dilution series of each mAb was preincubated with spike-pseudotyped lentiviruses for one hour at 37°C. The pre-incubated mAb:virus mixture was used to infect the cells in the plates

with each dilution point tested in technical replicate. After 48-55 hours, the media was removed from the plates, Bright-Glo reagent (Promega) was added and RLUs were measured. Data was analyzed and plotted GraphPad Prism (v9). Background signal from negative control wells was subtracted, replicate experiments were averaged, and the fraction of infectivity was calculated. and the half maximal inhibitory concentrations (IC50s) for the mAbs were calculated with a non-linear regression fit for inhibition versus response constraining the bottom to 0, the top to 1, and HillSlope < 0. Similarly, the plasma neutralizing titer (NT50), the reciprocal dilution factor for 50% neutralization, was calculated with a non-linear fit for inhibition versus response constraining the bottom to 0, the top to 1, and the HillSlope > 0. The geometric mean of the IC50s and 95% confidence intervals across authentic SARS-CoV-2 VOCs tested with IC50 >10000 ng/mL set to 10000 ng/mL this calculation.

Authentic SARS-CoV-2 microneutralization assay

One day prior to infection, $2x10^4$ Vero E6-TMPRSS2 cells per well were seeded in 96-well luminometer-compatible tissue culture plates (Perkin Elmer) and incubated overnight. A dilution series of each mAb was generated with concentrations of 0.0316, 0.1, 0.316, 1, 3.16 and 10 μg/ml. 10^4 $TCID_{50}$/mL of authentic SARS-CoV-2 D614G, Alpha, Delta, BA.1, BA.4, or BA.2.12.1 virus (obtained from Laboratoire de santé publique du Québec) was prepared in DMEM + 2% FBS and combined with an equivalent volume of diluted mAbs for one hour. After this incubation, all media was removed from the 96-well plate seeded with Vero E6-TMPRSS2 cells and the virus:mAb mixture was added to each respective well at a volume corresponding to 600 $TCID_{50}$ per well. Both virus only and media only (DMEM + 2% FBS) conditions were included in this assay. After one hour incubation at 37°C, the virus:mAb supernatant was removed from wells, and each diluted mAb was added to its respective Vero E6-TMPRSS2-seeded well in addition to an equivalent volume of DMEM + 2% FBS and was then incubated for 48 hours. Media was then discarded and replaced with 10% formaldehyde for 24 hours to cross-link Vero E6-TMPRSS2 monolayer. Then, the plates were removed from BSL3+. Formaldehyde was removed from wells and subsequently washed with PBS. Cell monolayers were permeabilized for 15 minutes at room temperature with PBS + 0.1% Triton X-100, washed and then incubated for one hour at room temperature with PBS + 3% non-fat milk. A SARS-CoV-2 nucleocapsid protein monoclonal antibody (Bioss Antibodies, clone 1C7) solution was prepared at 1 μg/mL and added to all wells for one hour at room temperature. Following 4x

washes with PBS, an anti-mouse IgG HRP secondary antibody solution was applied. One-hour post-room temperature incubation, the plate was washed 4x with PBS, substrate (ECL) was added and an LB941 TriStar luminometer (Berthold Technologies) was used to measure the signal of each well. Data was analyzed and plotted using GraphPad Prism (v9). Background signal from negative control wells was subtracted, replicates averaged, and the percent infectivity was calculated. The half maximal inhibitory concentrations (IC50s) for the mAbs were calculated with a non-linear regression fit for inhibition versus response.

Yeast display deep mutational scanning

Yeast-display libraries containing virtually all single amino acid mutations in the Wuhan-Hu-1, Omicron BA.1, and Omicron BA.2 RBDs were used to identify escape mutations as previously described (17). Briefly, 5 OD of yeast libraries were incubated for one hour at room temperature with a concentration of antibody determined as the binding EC90 to parental RBD. In parallel, 0.5 OD of respective parental RBD constructs were incubated in 100 µL of antibody at the same EC90 concentration or 0.1x the concentration for calibrating FACS sort gates. Cells were washed, incubated with 1:100 FITC-conjugated chicken anti-Myc antibody (Immunology Consultants, clone CMYC-45F) to label for RBD expression and 1:200 PE-conjugated goat anti-human-IgG (Jackson ImmunoResearch, cat. 109-115-098) to label for bound mAb.

Antibody-escape cells in each library were selected via FACS on a BD FACSAria II. FACS selection gates were drawn to capture approximately 50% of yeast expressing the parental RBD labeled at 0.1x the EC90 library labeling concentration (see gates in **Fig. S8A**). For each sample, approximately 4 million RBD^+ cells were processed on the sorter with collection of cells in the antibody-escape bin. Sorted cells were grown overnight, plasmid purified, and mutant-identifier N16 barcodes sequenced on an Illumina NextSeq. All subsequent computational steps and intermediate data files are available at https://github.com/jbloomlab/SARS-CoV-2-RBD_Omicron_MAP_Overbaugh_v1/blob/main/results/summary/summary.md. Demultiplexed Illumina barcode reads were matched to library barcodes in barcode-mutant lookup tables using dms_variants (version 0.8.9), yielding a table of counts of each barcode in pre- and post-sort populations. The escape fraction of each barcoded variant was computed from sequencing counts in the pre-sort and antibody-escape populations via the formula:

$$E_v = F \times (n_v^{post}/N_{post}) \div (n_v^{pre}/N_{pre})$$

where *F* is the total fraction of the library that escapes antibody binding (numbers in **Fig. S8A**), n_v is the counts of variant *v* in the pre- or post-sort samples with a pseudocount addition of 0.5, and *N* is the total sequencing count across all variants pre- and post-sort. These escape fractions represent the estimated fraction of cells expressing a particular variant that fall in the escape bin. We applied computational filters to remove mutants with low pre-selection sequencing counts or highly deleterious mutations as described previously (18). Per-mutant escape fractions were computed as the average across barcodes within replicates, with the correlations between replicate library selections shown in **Fig. S8B,C**. Final escape fraction measurements averaged across two replicates are available from GitHub: https://github.com/jbloomlab/SARS-CoV-2-RBD_Omicron_MAP_Overbaugh_v1/blob/main/results/supp_data/Wuhan_Hu_1/all_mAbs_WH1_raw_data.csv ; https://github.com/jbloomlab/SARS-CoV-2-RBD_Omicron_MAP_Overbaugh_v1/blob/main/results/supp_data/Omicron_BA1/all_mAbs_BA1_raw_data.csv ; and https://github.com/jbloomlab/SARS-CoV-2-RBD_Omicron_MAP_Overbaugh_v1/blob/main/results/supp_data/Omicron_BA2/all_mAbs_BA2_raw_data.csv . Raw sequencing data for yeast-display deep mutational scanning experiments are on the NCBI SRA under BioProject PRJNA770094, BioSample SAMN34381850.

Lentivirus-based full spike deep mutational scanning

Omicron BA.1 spike deep mutational scanning libraries were designed to contain all functionally tolerated mutations at every position in spike as previously described (19). To identify mutations in BA.1 spike that would escape C68.59 antibody, we used the approach described in (19). Briefly, the spike-pseudotyped viral libraries were incubated for one hour at 37°C with increasing concentrations of C68.59 antibody, starting with IC99 concentration at 20.2 µg/ml and increasing this concentration by 4 and 16-fold. The library-antibody mix was used to infect the 293T-ACE2 cells described in (15). After infection, the viral barcodes were harvested and sequenced as described in (19). The escape conferred by each mutation was determined relative to a VSV-G pseudotyped neutralization standard as described in (19). This analysis used the biophysical model implemented in *polyclonal* package (https://jbloomlab.github.io/polyclonal/) (19). The computational pipeline used to

implement this analysis is at https://github.com/dms-vep/SARS-CoV-2_Omicron_BA.1_spike_DMS_C68.59, C68.59 escape sites analysis is documented at https://dms-vep.github.io/SARS-CoV-2_Omicron_BA.1_spike_DMS_C68.59/ and visualized at https://dms-vep.github.io/SARS-CoV-2_Omicron_BA.1_spike_DMS_C68.59/C68.59_escape_plot.html.

Sequence alignment

Amino acid sequences for SARS-CoV-2 VOCs and SARS-CoV-1 were obtained from the NIH NCBI Virus SARS-CoV-2 Data Hub (https://www.ncbi.nlm.nih.gov/labs/virus/vssi/#/). Sequences were aligned using MAFFT (v7, https://mafft.cbrc.jp/alignment/server/) (20) and visualized using Jalview (v2.11.2.5) (21).

Protein expression and purification for BLI, HDX, and cryo-EM

Wuhan-Hu-1 Spike containing the 'HexaPro' (6P) stabilizing mutations (22) was produced by transient transfection of Expi293F cells; the SARS-CoV-2 S 6P expression vector was a gift from Jason McLellan (Addgene plasmid #154754). The secreted protein was captured by Strep-Tactin affinity chromatography, digested overnight at room temperature with HRV 3C protease (ThermoFisher) to remove the affinity tag, and purified by size-exclusion chromatography on a Superose 6 Increase column (Cytiva) in 10mM HEPES, pH 7.4, 250mM NaCl, 0.02% sodium azide. Protein was stored at 4°C.

Purified C68.59 IgG was digested into Fab fragments using a Pierce™ Fab Preparation Kit (Thermo Fisher) according to manufacturer's instructions. Prior to experiments both Fab and 6P spike were buffer-exchanged into HEPES-buffered saline (HBS, pH 7.4) using Zeba spin columns (ThermoFisher).

Cryo-EM Data Processing

Movies were motion-corrected and binned by 2 using MotionCor2. Particles were picked manually from 20 micrographs and used to train a convolutional neural network to perform automated particle picking using crYOLO (23), resulting in an initial set of 604,558 particles. CTF estimation, and all further steps were carried out using Relion-4.0 (24). Particles were extracted with a box size of 120 pixels, binned to 3.336 Å/pixel. 2D class averaging was performed using the VDAM algorithm for 200 iterations with a mask diameter of 250 Å, separated into 100 classes with regularization parameter T=2. Classes not resembling protein density were manually excluded, and the remaining particles were used for initial model generation with 200 iterations of the

VDAM algorithm, mask diameter 250 Å, and regularization parameter T=4. The resulting initial model was used as a reference for gold standard refinement using 3D-autorefine with C3 symmetry applied. 3D classification was then performed with 5 classes for 25 iterations. Classes resembling S6P with no additional density were combined and refined individually using 3D-autorefine, and the remaining classes were combined and once again subject to 3D classification with 5 classes for 25 iterations. The resulting classes contained additional density at the spike binding site and were combined into 2 sets depending on whether the S6P appeared to exhibit a native or disrupted structure, and both sets were refined individually using 3D-autorefine. Resolution was estimated using FSC=0.143 criterion during Relion post-processing, and local resolution was calculated using ResMap (25). UCSF Chimera (26) and ChimeraX (27) were used for visualization.

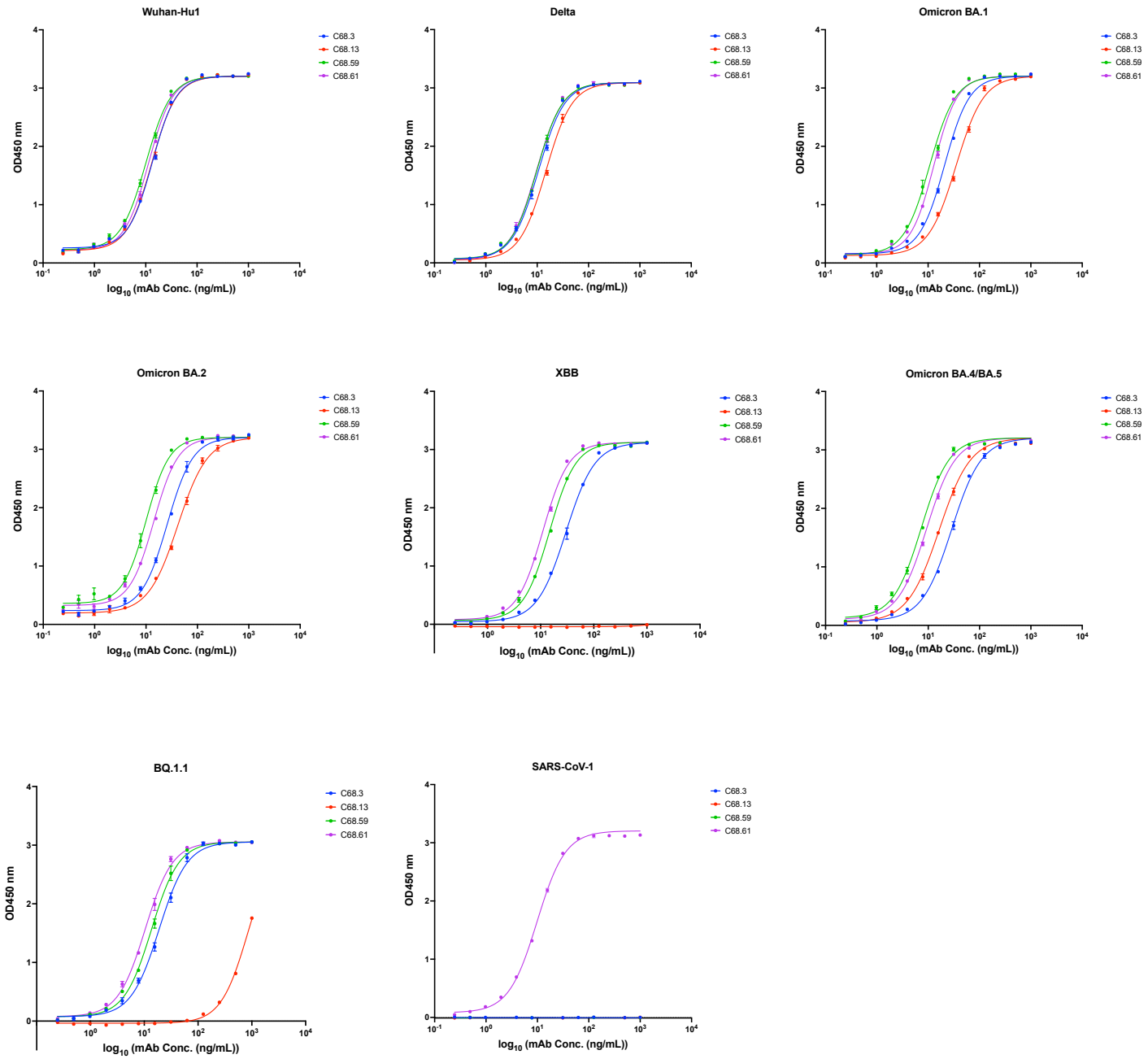

Fig. S1. Binding curves for four C68 mAbs to spike trimers from SARS-CoV-2 VOCs and SARS-CoV-1. Binding of C68 mAbs (C68.3, blue; C68.13, red; C68.59, green; C68.61, purple) to recombinant spike trimers from SARS-CoV-2 Wuhan-Hu-1 (WH-1), SARS-CoV-2 VOCs (Delta, Omicron BA.1, Omicron BA.2, Omicron XBB, Omicron BA.4/BA.5, Omicron BQ.1.1) or SARS-CoV-1. The concentration of each mAb (ng/mL) is plotted on a $\log_{10}$ scale versus absorbance (OD450 nm). All C68 mAbs reached maximal absorbance and bound strongly to the SARS-CoV-2 VOCs, except C68.13 in with XBB and BQ.1.1 spikes. C68.61 was the only C68 mAb to bind

SARS-CoV-1 spike trimer. Data (mean ± SEM) are shown from a representative experiment with two technical replicates. Curves are non-linear regression fits of the average of the replicates.

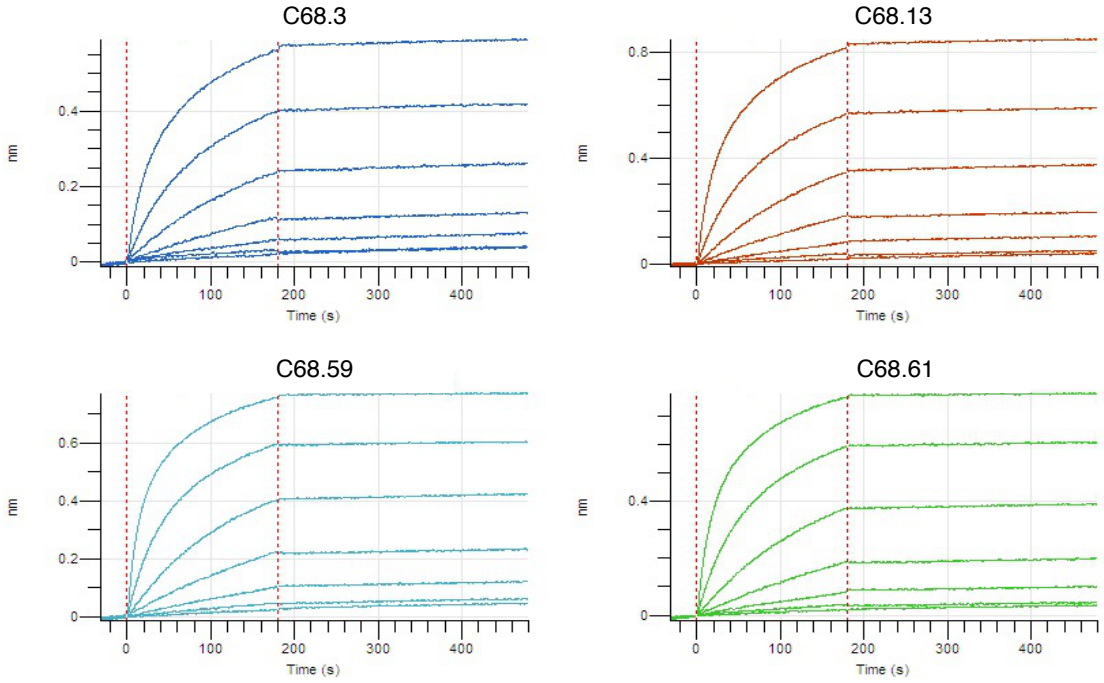

Fig. S2. Biolayer interferometry (BLI) sensograms measuring binding of C68 mAbs to stabilized WH-1 spike trimer. IgG loaded tips were dipped into a 3-fold dilution series of WH-1 spike with the "HexaPro" mutations (6P) at 25°C, pH 7.4, starting at 200nM concentration. IgGs of C68.3 (blue, top left), C68.13 (orange, top right), C68.59 (teal, bottom left), C68.61 (green, bottom right) were tested. All mAbs bound very tightly and exhibited slow off rates making quantification of binding kinetics unreliable.

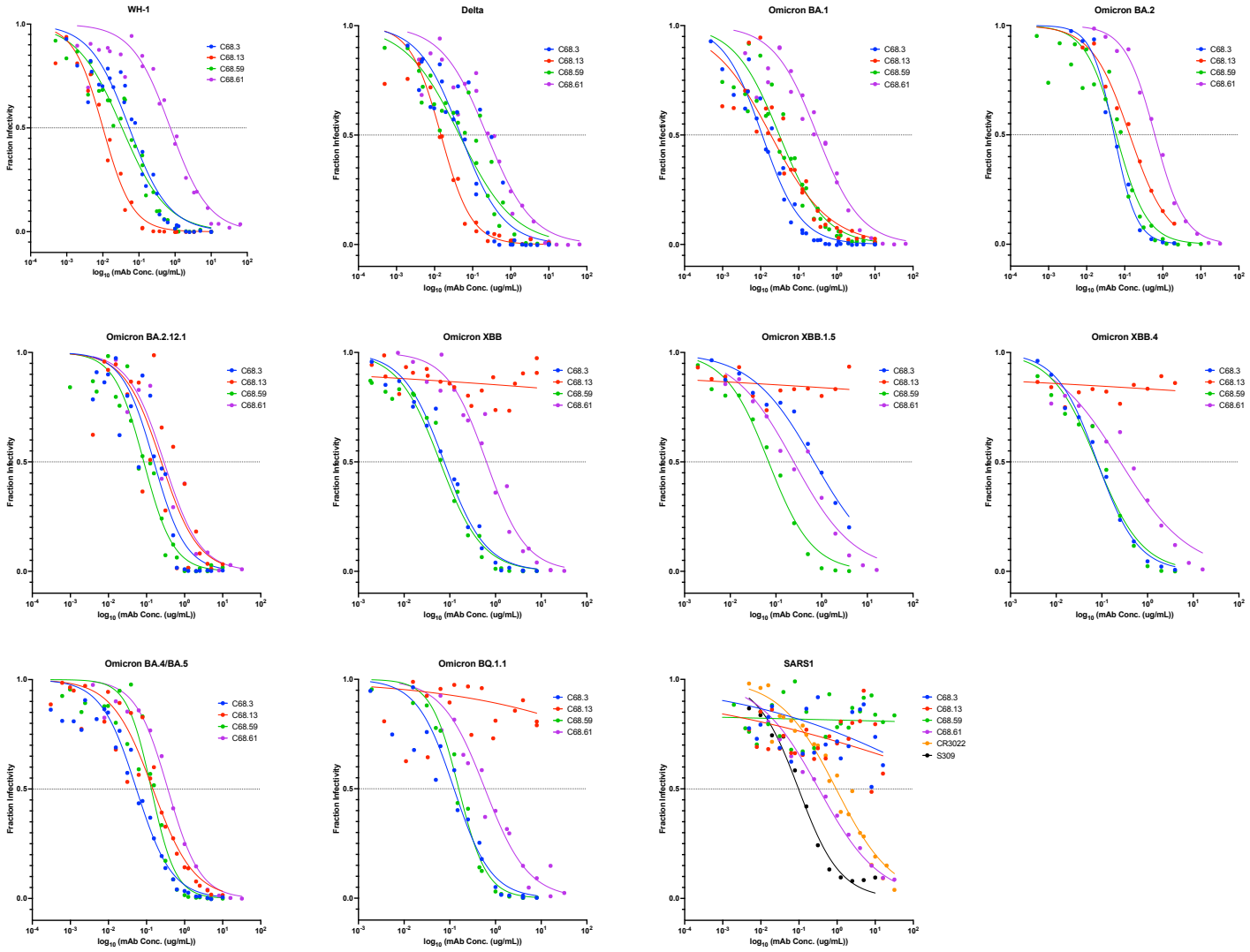

Fig. S3. Neutralization curves of four novel C68 mAbs against SARS-CoV-2 VOC and SARS-CoV-1 spike-pseudotyped lentiviruses. Neutralization of the following spike-pseudotyped lentiviruses were assessed: Wuhan-Hu-1 (WH-1), Delta, Omicron variants BA.1, BA.2, BA.2.12.1, XBB, XBB.1.5, XBB.4, BA.4/BA.5, BQ.1.1 and SARS-CoV-1 (SARS1). Each pseudovirus was incubated with increasing concentrations of C68 mAbs individually before infecting HEK293-ACE2 cells. In each graph, fraction infectivity is shown for C68.3 (blue), C68.13 (red), C68.59 (green), and C68.61 (purple) with mAb concentration (μg/mL) plotted on a $\log_{10}$ scale. Curves are non-linear regression fits of the average of independent experiments. All C68 mAbs were tested in at least three independent experiments per pseudovirus, each with technical replicates, in two different

pseudovirus batches. In the SARS-CoV-1 experiment, S309 (black) and CR3022 (orange) were run as well in duplicate experiments with technical replicates. The dashed lines indicate fraction infectivity = 0.5.

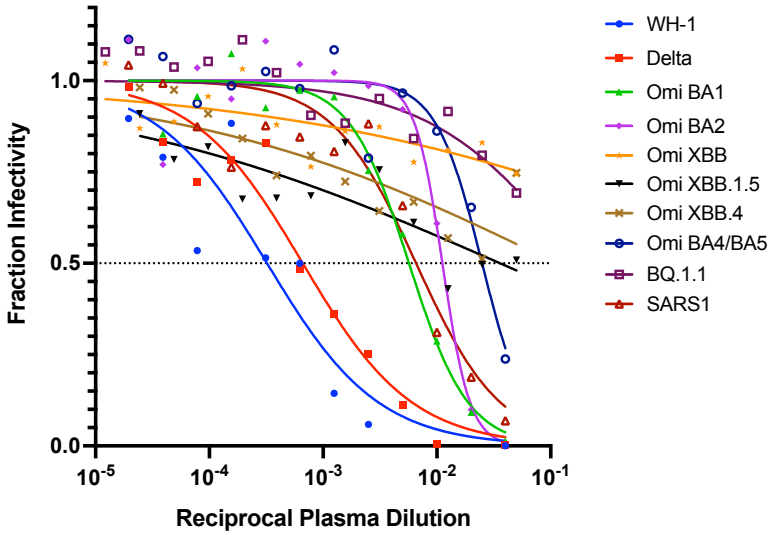

	WH-1	Delta	Omi BA.1	Omi BA.2	Omi XBB	Omi XBB.1.5	Omi XBB.4	Omi BA.4/5	Omi BQ.1.1	SARS-CoV-1
NT50	2318	2613	875	146	<10	28	<10	40	<10	152

Fig. S4. Neutralization activity of 30-day post symptom onset plasma against SARS-CoV-2 VOCs and SARS-CoV-1. Neutralization was measured using a spike-pseudotyped lentivirus assay in HEK293T-ACE2 cells. Neutralization curves (non-linear regression fit) for C68 plasma against Wuhan-Hu-1 (WH-1, blue); Delta (red); Omicron BA.1 (green); Omicron BA.2 (purple); Omicron XBB (orange), Omicron XBB.1.5 (black), Omicron XBB.4 (brown), Omicron BA.4/BA.5 (dark blue), Omicron BQ.1.1 (maroon), and SARS-CoV-1 (SARS1, red) pseudotyped viruses are shown with plasma dilution factor plotted on a $\log_{10}$ scale. NT50 were calculated as the reciprocal dilution factor of the plasma that gives the half-maximal pseudotyped virus neutralization. Curves are non-linear regression fits. Data shown for WH-1, Delta, Omicron BA.1 and BA.2 are the average of two independent experiments, each with two technical replicates. The remaining curves are the average of two technical replicates in one experiment. The dashed line indicates 0.5 fraction infectivity.

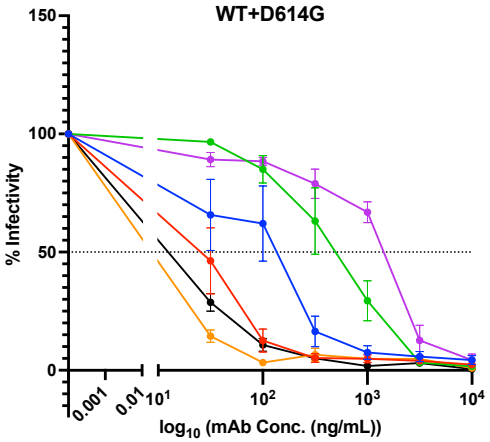
WT+D614G
% Infectivity
150
100
50
0
0.001
0.01
10^1
10^2
10^3
10^4
$\log_{10}$ (mAb Conc. (ng/mL))

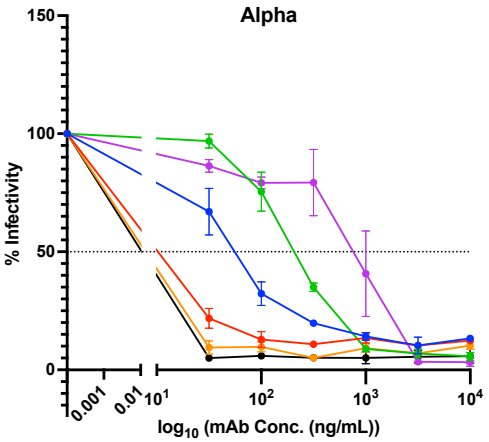
Alpha
% Infectivity
150
100
50
0
0.001
0.01
10^1
10^2
10^3
10^4
$\log_{10}$ (mAb Conc. (ng/mL))

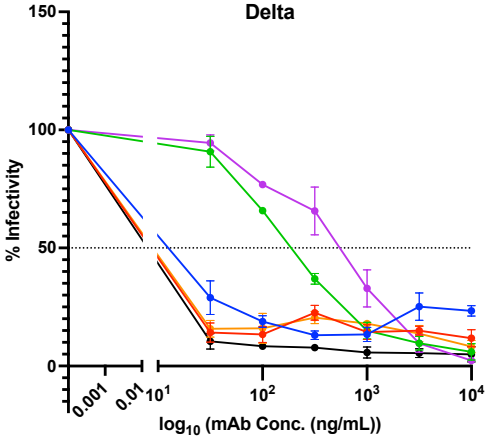
Delta
% Infectivity
150
100
50
0
0.001
0.01
10^1
10^2
10^3
10^4
$\log_{10}$ (mAb Conc. (ng/mL))

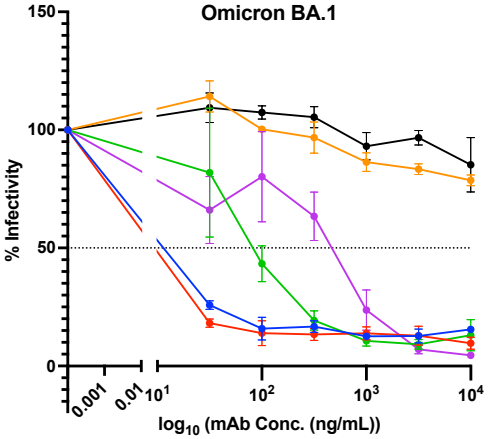
Omicron BA.1
% Infectivity
150
100
50
0
0.001
0.01
10^1
10^2
10^3
10^4
$\log_{10}$ (mAb Conc. (ng/mL))

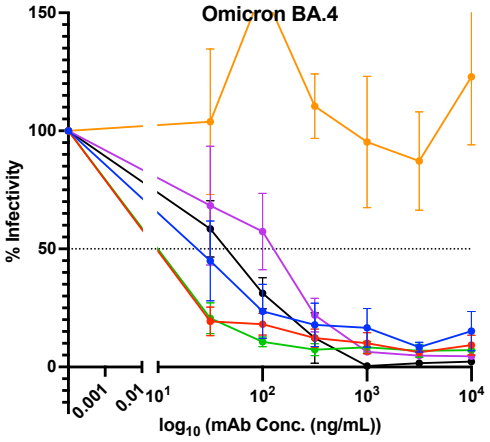
Omicron BA.4
% Infectivity
150
100
50
0
0.001
0.01
10^1
10^2
10^3
10^4
$\log_{10}$ (mAb Conc. (ng/mL))

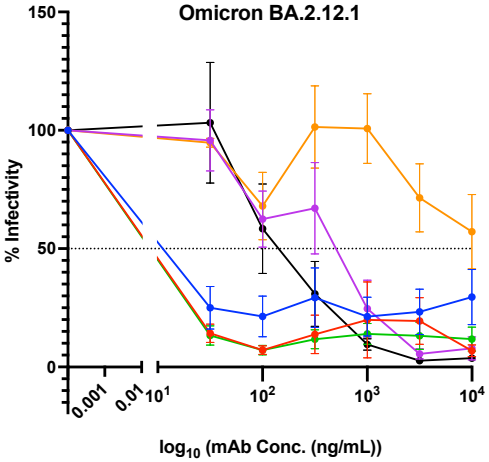
Omicron BA.2.12.1
% Infectivity
150
100
50
0
0.001
0.01
10^1
10^2
10^3
10^4
$\log_{10}$ (mAb Conc. (ng/mL))

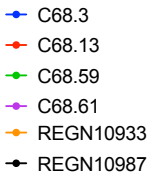
C68.3
C68.13
C68.59
C68.61
REGN10933
REGN10987

Fig. S5. Neutralization activity of four C68 mAbs against authentic SARS-CoV-2 variant viruses. Neutralization curves for Wuhan-Hu-1 with D614G mutation (WT+D614G), Alpha, Delta, Omicron BA.1, Omicron BA.4, and Omicron BA.2.12.1 viruses. The percent infectivity of each virus in VERO-E6-TMPRSS2 cells after incubation with increasing concentrations of mAb (ng/mL) plotted on a $\log_{10}$ scale. The following mAbs were assessed: C68.3 (blue), C68.13 (red), C68.59 (green), C68.61 (purple), including two previously approved therapeutic mAbs (REGN10933 (orange), REGN10987 (black)) for comparison. Delta and Alpha authentic virus neutralizations were run with three technical replates in one experiment, the other viruses were tested in two independent experiments, each with three technical replicates. For each data point, the mean $\pm$ the SEM are shown. These data were used to calculate the half maximal inhibitory concentrations (IC50s) for the mAbs with a non-linear regression fit for inhibition versus response.

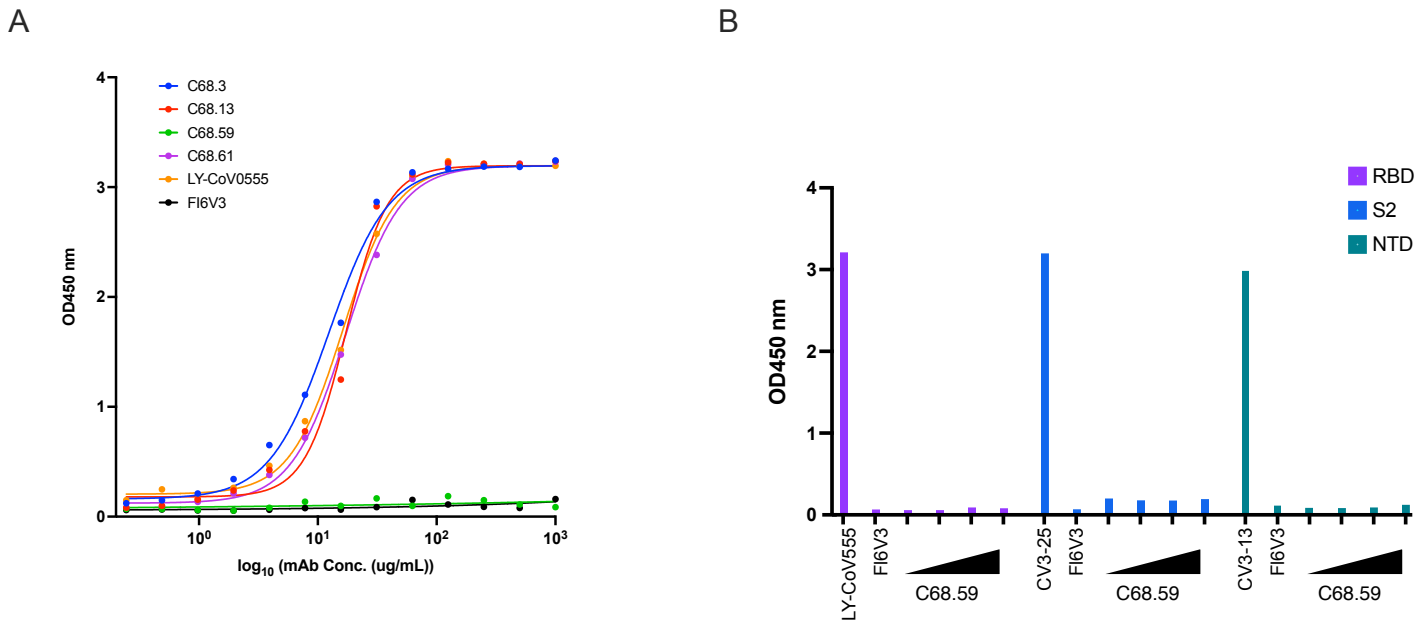

Fig. S6. Binding assessment of C68 mAbs against subunits of spike glycoprotein. (A) Binding of C68.3 (blue), C68.13 (red), C68.59 (green), and C68.61 (purple) to WH-1 RBD peptide measured by absorbance at OD450 nm with increasing amounts of mAb (ug/mL). A positive control (LY-CoV555, orange) and a negative control (influenza mAb FI6V3, black) were run in parallel. All of the C68 mAbs bound strongly to WH-1 RBD except C68.59, which had no binding. Data shown are from a single experiment with technical replicates. Curves are non-linear regression fits of the average of the replicates. (B) Binding (OD450 nm) of C68.59 to peptides representing spike regions RBD (purple), S2 (blue), and NTD (green) at increasing concentrations of mAb (2 μg/mL, 12.5 μg/mL, 25 μg/mL, 50 μg/mL). mAbs with known spike epitopes were included as positive controls at 2μg/mL: LY-CoV555 (RBD-specific), CV3-25 (S2-specific)(11), CV3-13 (NTD-specific)(12). The influenza antibody FI6V3 was included as a negative control. C68.59 did not bind to RBD, NTD, or S2 even at 50 μg/mL.

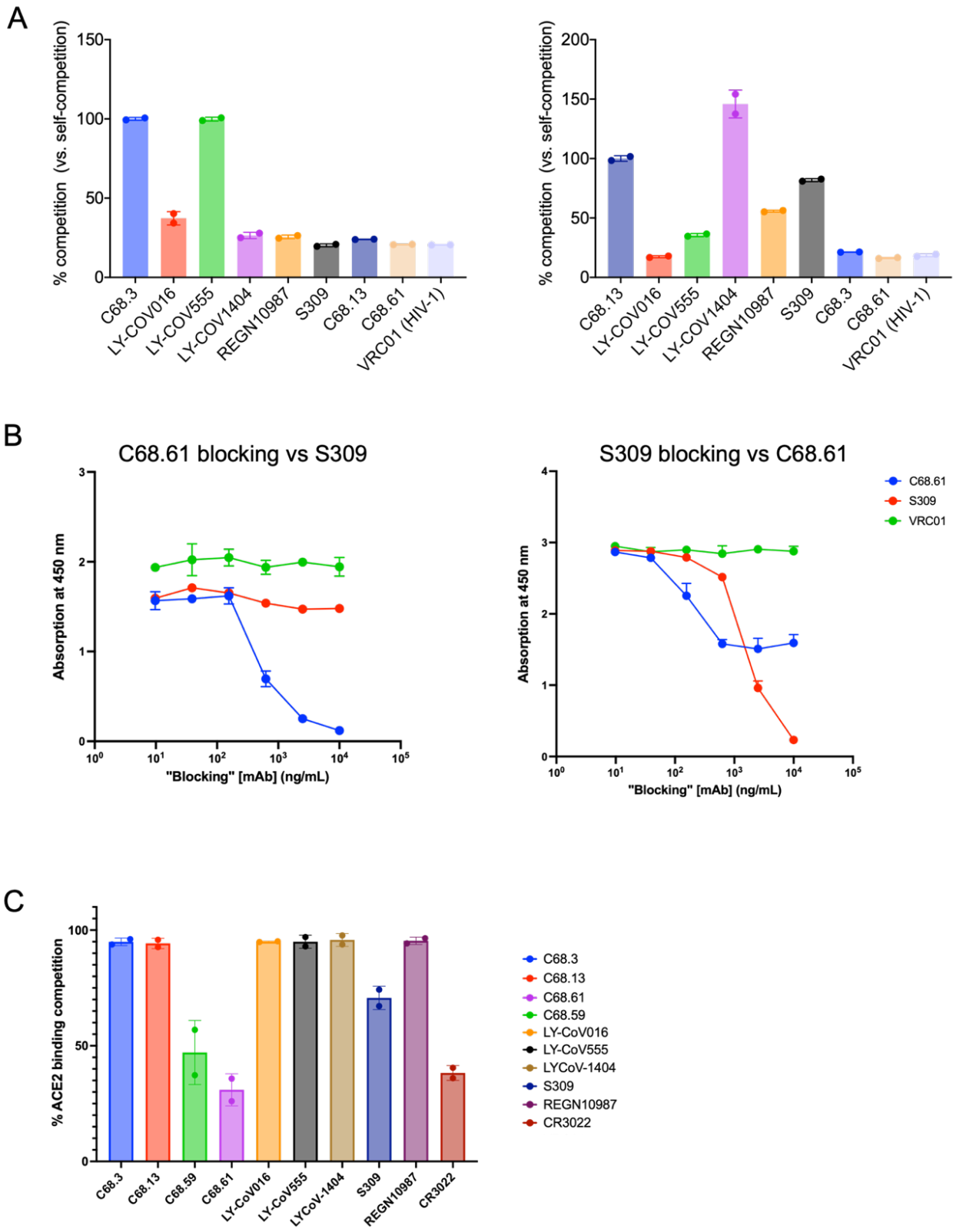
A
% competition (vs. self-competition)
150
100
50
0
C68.3
LY-COV016
LY-COV555
LY-COV1404
REGN10987
S309
C68.13
C68.61
VRC01 (HIV-1)
% competition (vs. self-competition)
200
150
100
50
0
C68.13
LY-COV016
LY-COV555
LY-COV1404
REGN10987
S309
C68.3
C68.61
VRC01 (HIV-1)
B
C68.61 blocking vs S309
Absorption at 450 nm
"Blocking" [mAb] (ng/mL)
S309 blocking vs C68.61
Absorption at 450 nm
"Blocking" [mAb] (ng/mL)
C68.61
S309
VRC01
C
% ACE2 binding competition
100
50
0
C68.3
C68.13
C68.59
C68.61
LY-CoV016
LY-CoV555
LYCoV-1404
S309
REGN10987
CR3022
C68.3
C68.13
C68.61
C68.59
LY-CoV016
LY-CoV555
LYCoV-1404
S309
REGN10987
CR3022

Fig. S7. Competition ELISAs to map RBD epitope classes and ACE2-binding inhibition. (A) Bar graphs showing the percent competition of commercial mAbs against C68.3 (left) and C68.13 (right). Binding to prefusion-stabilized WH-1 spike glycoprotein was performed with each biotinylated competitive C68 mAbs in the presence of "blocking" commercial mAb. To confirm competition, all assays were run in reverse with non-biotinylated C68 mAb competed with biotinylated commercial mAb. These commercial mAbs were selected because they represent different classes of RBD-specific mAbs: LY-CoV016 (Class 1), LY-CoV555 (Class 2), LY-CoV1404 (Class 2/3), REGN10987 (Class 3), S309 (Class 3). For each mAb, percent competition was calculated using area under the curve (AUC) of each dilution series with respect to the self-competition condition. HIV-1-specific VRC01 was included as a negative control. The means and ±SD are plotted. Self-competition is set to 100% for each mAb. All experiments were run with two technical replicates. (B) Competition ELISA dilution curves of blocking mAbs C68.61 (left) and S309 (right) with biotinylated mAbs C68.61 (blue), S309 (red) and VRC01 (negative control). In both graphs, self-competition results in a reduction of fluorescent signal (absorption at OD450 nm) with increasing concentration of blocking mAb (ng/mL) plotted as a $\log_{10}$ scale on the x axis. When blocking with S309, a similar reduction in fluorescent is seen with biotinylated C68.61 (right) as with self-competition indicating competition between the two mAbs, but this completion was unidirectional. The means and ±SD are plotted as averages of two technical replicates in a single experiment (C) Assessment of ACE2 inhibition by mAb binding using competition ELISAs. Bar graphs show the average percent inhibition ±SD across two independent experiments each with two technical replicates. Several positive control, commercial mAbs that are known to inhibit ACE2 binding were included for comparison. VRC01 was run as a negative control.

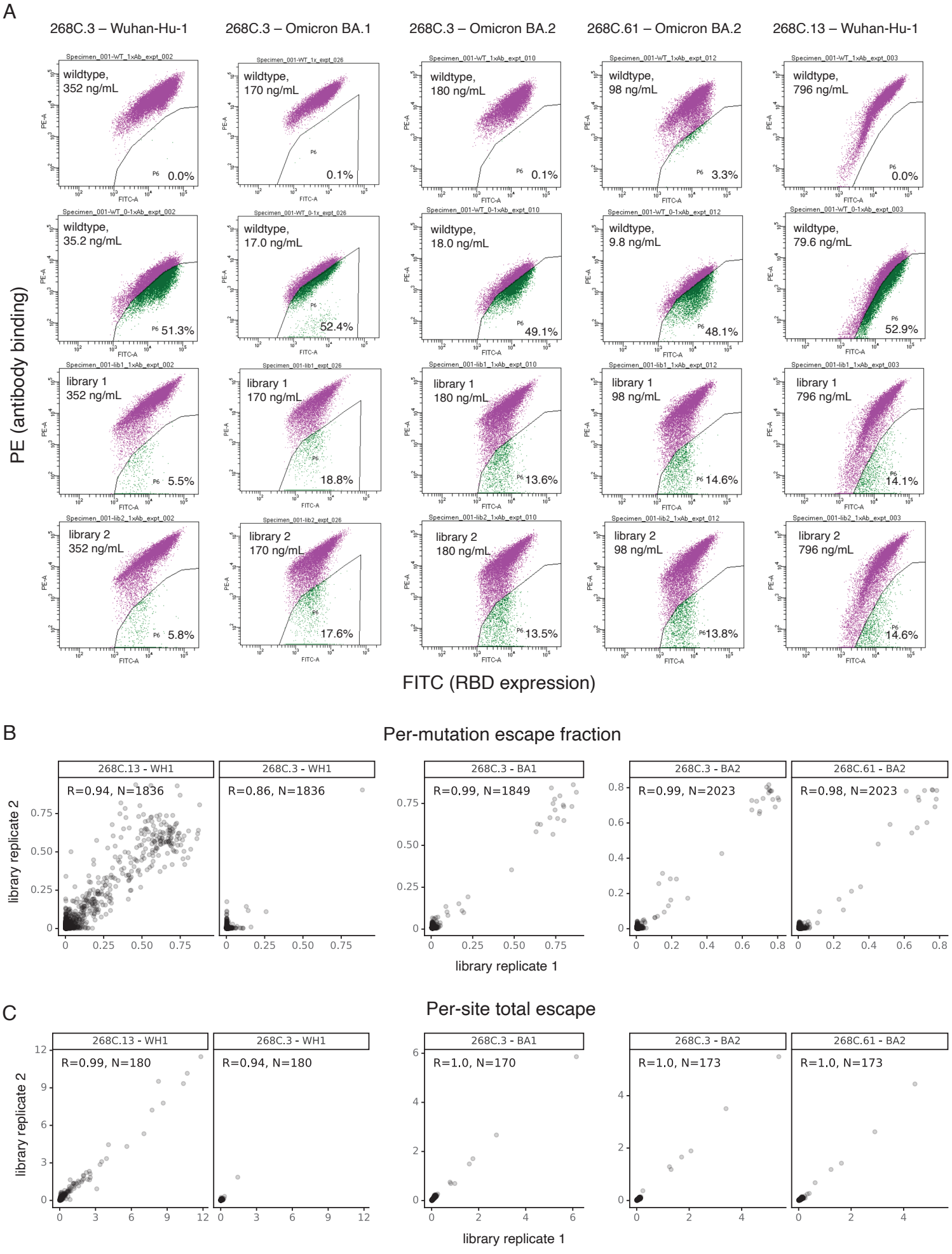
A
268C.3 – Wuhan-Hu-1
268C.3 – Omicron BA.1
268C.3 – Omicron BA.2
268C.61 – Omicron BA.2
268C.13 – Wuhan-Hu-1
wildtype, 352 ng/mL
0.0%
wildtype, 170 ng/mL
0.1%
wildtype, 180 ng/mL
0.1%
wildtype, 98 ng/mL
3.3%
wildtype, 796 ng/mL
0.0%
wildtype, 35.2 ng/mL
51.3%
wildtype, 17.0 ng/mL
52.4%
wildtype, 18.0 ng/mL
49.1%
wildtype, 9.8 ng/mL
48.1%
wildtype, 79.6 ng/mL
52.9%
library 1 352 ng/mL
5.5%
library 1 170 ng/mL
18.8%
library 1 180 ng/mL
13.6%
library 1 98 ng/mL
14.6%
library 1 796 ng/mL
14.1%
library 2 352 ng/mL
5.8%
library 2 170 ng/mL
17.6%
library 2 180 ng/mL
13.5%
library 2 98 ng/mL
13.8%
library 2 796 ng/mL
14.6%
PE (antibody binding)
FITC (RBD expression)
B
Per-mutation escape fraction
268C.13 - WH1
R=0.94, N=1836
268C.3 - WH1
R=0.86, N=1836
268C.3 - BA1
R=0.99, N=1849
268C.3 - BA2
R=0.99, N=2023
268C.61 - BA2
R=0.98, N=2023
library replicate 2
library replicate 1
C
Per-site total escape
268C.13 - WH1
R=0.99, N=180
268C.3 - WH1
R=0.94, N=180
268C.3 - BA1
R=1.0, N=170
268C.3 - BA2
R=1.0, N=173
268C.61 - BA2
R=1.0, N=173
library replicate 2
library replicate 1

Fig. S8. Yeast display deep mutational scanning gating scheme and quality control check on replicate runs in independently generated libraries. (A) FACS gates used to identify mutations that escape mAb binding. For each experiment, an antibody-escape gate was drawn to capture approximately 50% of cells in the respective wildtype control labeled at 0.1x the library selection concentration. The “escape fraction” represents the fraction of cells of a mutant genotype that fall into this antibody-escape sort bin with replicates compared on each axis. (B, C) For each experiment, the correlation in per-mutation escape fraction (B) or the sum of escape fractions of all mutations at a site (C).

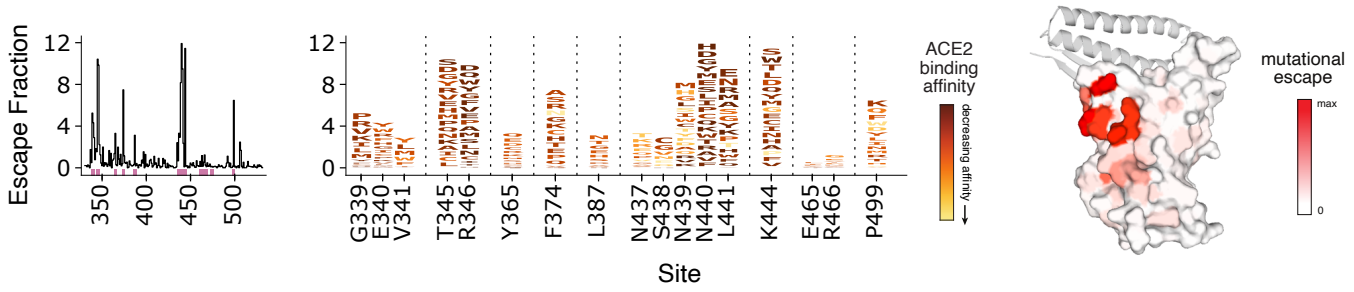

Fig. S9. RBD binding escape profile from DMS for C68.13. Line plot (left) identifies sites of binding escape (quantified as the sum of the escape fractions) at each site in the WH-1 library. Escape fractions were averaged across the two replicates in independently generated libraries. Sites that have strong escape mutations (high escape fractions) are marked with pink boxes under the plots and are represented in the logo plots (right). The logo plots showing the mutations that confer escape at each of these sites where the size of the amino acid letters are scaled according to the contribution to the overall escape fraction, and the color of the mutations indicates the effect of that mutation on ACE2 binding in the WH-1 background using previously published data profiling ACE2 escape profiles in the same yeast RBD display DMS system (17, 18). Yellow mutations indicate a deleterious effect that decreases ACE2 affinity and dark red indicates increased binding of that mutation on ACE2 compared to the wildtype amino acid. On the right, sites of escape for C68.13 are mapped on the RBD structure (space filled) bound to ACE2 (ribbons). The intensity of the red coloring is scaled according to the magnitude of the mutational escape fraction at each residue with white representing no change in binding between the wildtype and mutant amino acids at that site. Sites with the highest mutation escape fractions (darkest red) suggest key binding residues in the mAb epitope.

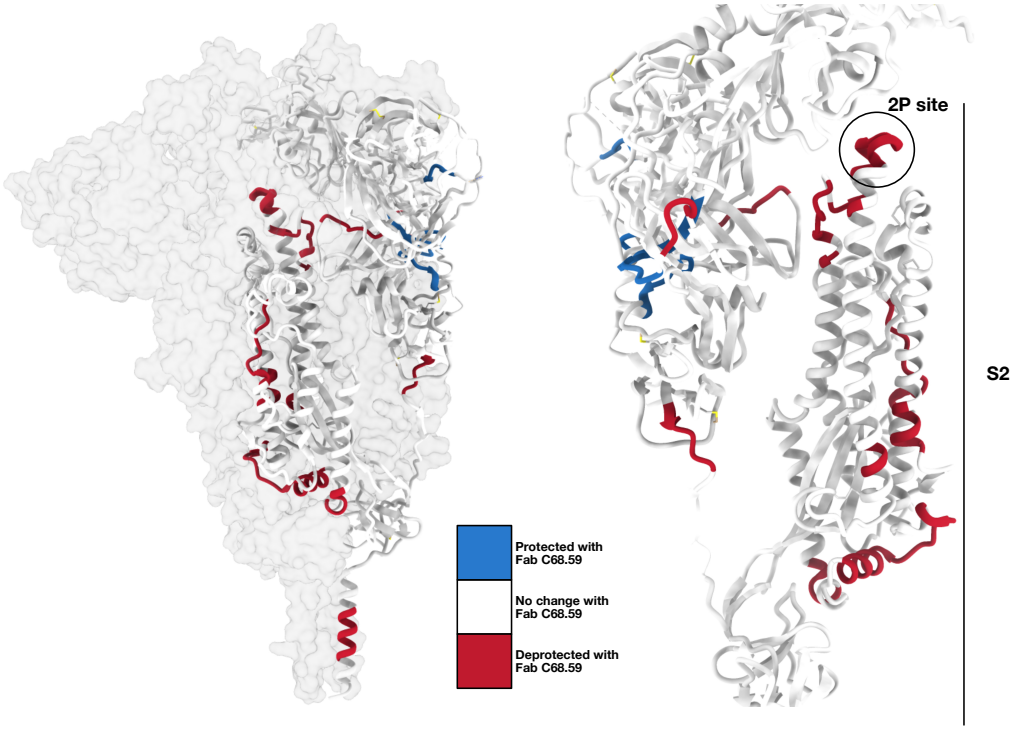

Fig. S10. Overall impact of C68.59 Fab binding to spike trimer mapped by HDX-MS. (A) Differential HDX displayed on the spike trimer structure (PDB ID 7SBP); red indicates an increase in uptake in the presence of C68.59, blue indicates a decrease, white indicates no significant change. (B) Monomer view of the same structure showing the S2 subunit, including the '2P' stabilizing mutation site.

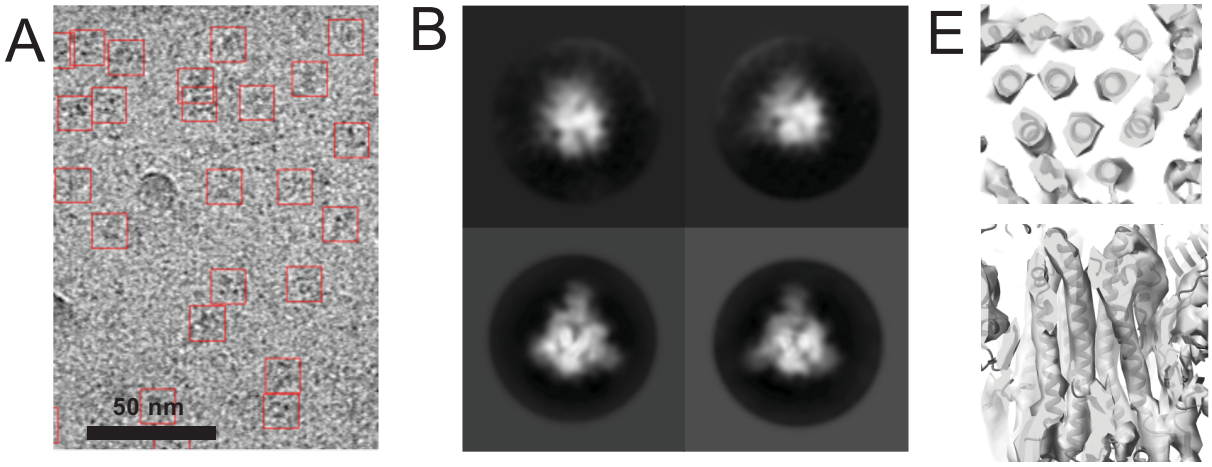
A
50 nm
B
E

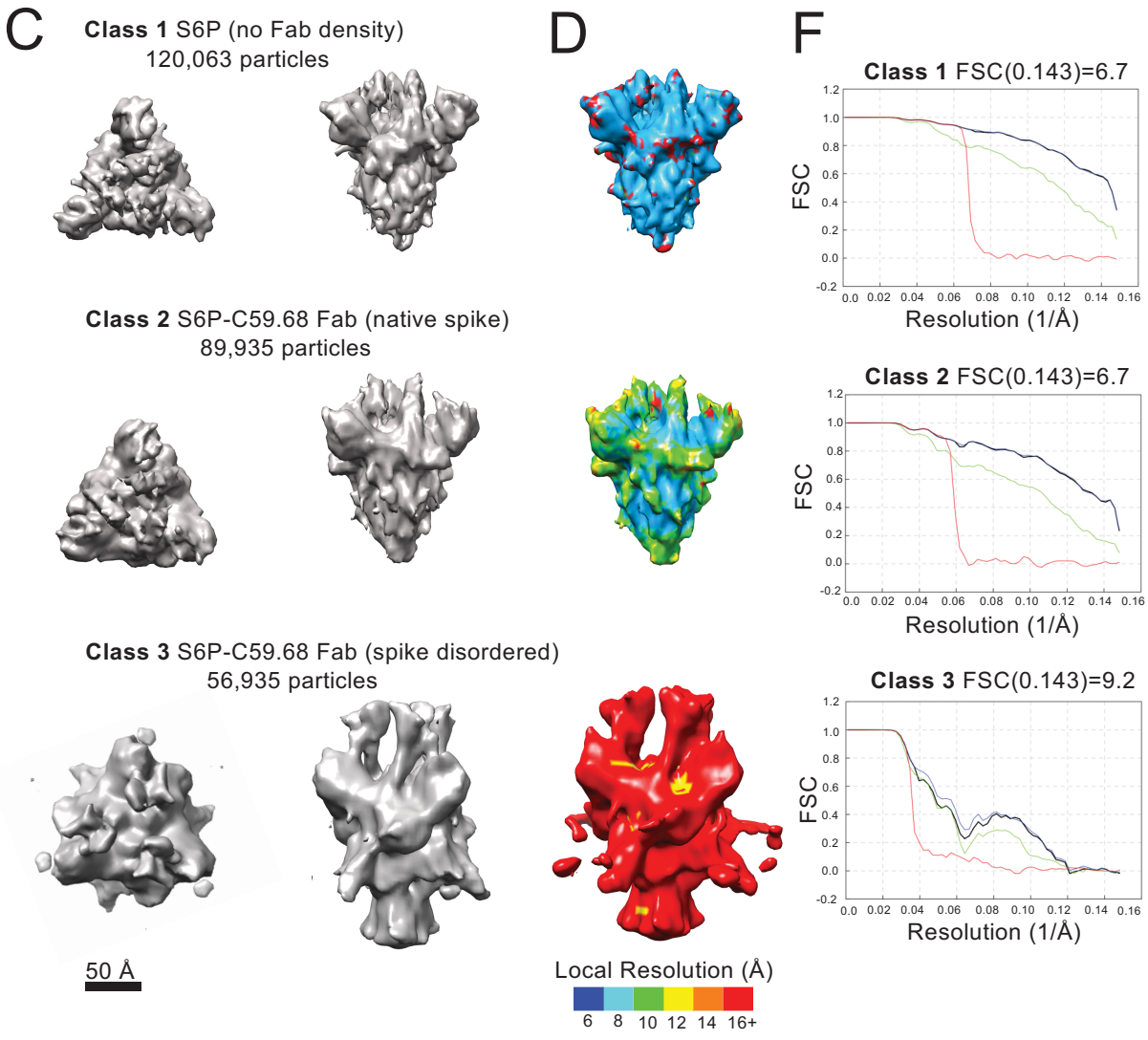
C
Class 1 S6P (no Fab density)
120,063 particles
Class 2 S6P-C59.68 Fab (native spike)
89,935 particles
Class 3 S6P-C59.68 Fab (spike disordered)
56,935 particles
50 Å
D
Local Resolution (Å)
6 8 10 12 14 16+
F
Class 1 FSC(0.143)=6.7
Class 2 FSC(0.143)=6.7
Class 3 FSC(0.143)=9.2
FSC
Resolution (1/Å)

Fig. S11. Cryo-EM data processing and validation. (A) Representative electron micrograph (cropped) with particles picked by crYOLO contained in red boxes (Scale bar 50 nm) and (B) 2D class averages. (C) Representative views of volumes reconstructed after 3D classification. Scale bar 50 Å. (D) Reconstructed maps colored by local resolution for each class. Blue = 6.0 Å; Cyan = 8.0 Å; Green = 10.0 Å; Yellow = 12.0 Å, Orange = 14. Å; Red = >16 Å. (E) Gold standard Fourier shell correlation (FSC) for each class, calculated in Relion post-processing. FSC=0.143 cutoff for each map displayed above plot. Red line = corrected, phase randomized, masked FSC; Blue line = masked FSC; Black line = corrected, masked FSC; Green line = unmasked FSC. For panels (C-E), top row = S6P class exhibiting no Fab density; second row = S6P-C59.68 Fab structure in which S6P exhibits an ordered, native conformation; bottom row = S6P-C59.68 Fab structure in which S6P exhibits a non-native, disrupted range of conformations.

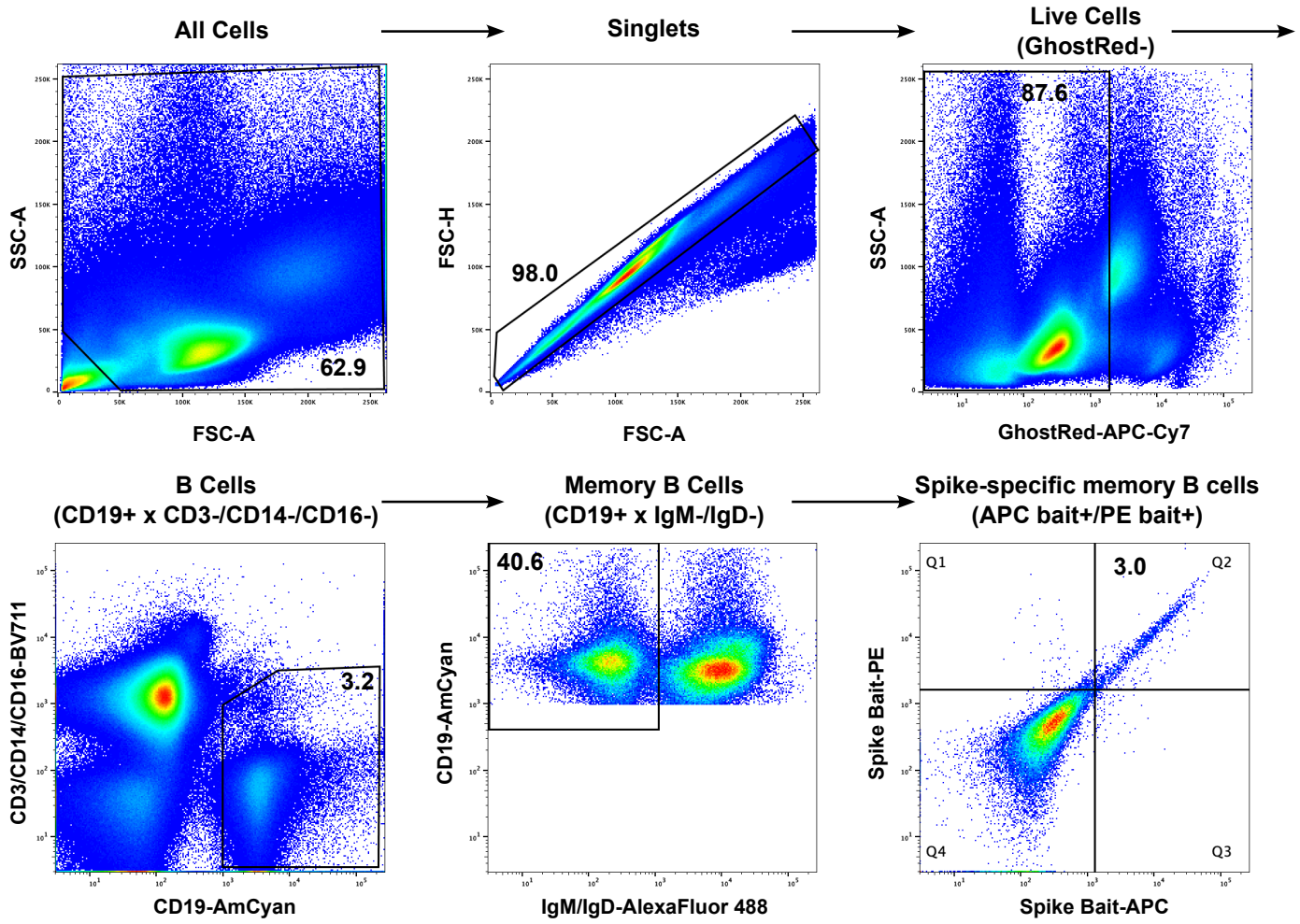

Fig. S12. Gating strategy for isolating Spike-specific memory B cells. A nested gating strategy is shown to isolate $CD3^{-}CD14^{-}CD16^{-}CD19^{+}IgD^{-}IgM^{-}$ memory B cells that were also double positive for "bait" (APC^{+} and PE^{+}, Q2 in final graph). The bait included Delta Spike Trimer and WH-1 S2 protein. These memory B cells were isolated from a sample of PBMCs collected from an individual 30-day post symptom onset of a Delta breakthrough infection.

Table S1. Cryo-EM Collection, Refinement, and Validation.

	Class 1 S6P	**Class 2** S6P-Fab	**Class 1** S6P-Fab (disordered)
Magnification	105,000x	105,000x	105,000x
Voltage (kV)	300	300	300
Electron exposure (e-/Å^2)	50	50	50
Defocus range (um)	0.7-0.12	0.7-0.12	0.7-0.12
Pixel Size (Å)	0.417	0.417	0.417
Symmetry imposed	C3	C3	C3
Initial Particle Images	604,558	604,558	604,558
Final Particle Images	120,063	89,935	59,935
Map Resolution (Å)	6.7	6.7	9.2
FSC threshold	0.143	0.143	0.143

SI References

1. C. A. Simonich *et al.*, HIV-1 Neutralizing Antibodies with Limited Hypermutation from an Infant. *Cell* **166**, 77-87 (2016).
2. C. A. Simonich *et al.*, A diverse collection of B cells responded to HIV infection in infant BG505. *Cell Rep Med* https://doi.org/10.1016/j.xcrm.2021.100314, 100314 (2021).
3. T. Tiller *et al.*, Efficient generation of monoclonal antibodies from single human B cells by single cell RT-PCR and expression vector cloning. *Journal of Immunological Methods* **329**, 112-124 (2008).
4. H. X. Liao *et al.*, High-throughput isolation of immunoglobulin genes from single human B cells and expression as monoclonal antibodies. *J Virol Methods* **158**, 171-179 (2009).
5. M. P. Lefranc *et al.*, IMGT, the international ImMunoGeneTics information system. *Nucleic Acids Res* **37**, D1006-1012 (2009).
6. K. L. Williams *et al.*, HIV-specific CD4-induced Antibodies Mediate Broad and Potent Antibody-dependent Cellular Cytotoxicity Activity and Are Commonly Detected in Plasma From HIV-infected humans. *EBioMedicine* **2**, 1464-1477 (2015).
7. E. M. Scherer *et al.*, Characteristics of memory B cells elicited by a highly efficacious HPV vaccine in subjects with no pre-existing immunity. *PLoS Pathog* **10**, e1004461 (2014).
8. M. M. Shipley *et al.*, Functional development of a V3/glycan-specific broadly neutralizing antibody isolated from a case of HIV superinfection. *Elife* **10** (2021).
9. H. L. Itell *et al.*, SARS-CoV-2 Antibody Binding and Neutralization in Dried Blood Spot Eluates and Paired Plasma. *Microbiol Spectr* **9**, e0129821 (2021).
10. M. E. Garrett *et al.*, High-resolution profiling of pathways of escape for SARS-CoV-2 spike-binding antibodies. *Cell* 10.1016/j.cell.2021.04.045 (2021).
11. W. Li *et al.*, Structural basis and mode of action for two broadly neutralizing antibodies against SARS-CoV-2 emerging variants of concern. *Cell Rep* **38**, 110210 (2022).
12. G. Beaudoin-Bussieres *et al.*, A Fc-enhanced NTD-binding non-neutralizing antibody delays virus spread and synergizes with a nAb to protect mice from lethal SARS-CoV-2 infection. *Cell Rep* **38**, 110368 (2022).
13. K. L. Williams *et al.*, Identification of HIV gp41-specific antibodies that mediate killing of infected cells. *PLoS Pathog* **15**, e1007572 (2019).
14. K. Westendorf *et al.*, LY-CoV1404 (bebtelovimab) potently neutralizes SARS-CoV-2 variants. *Cell Rep* **39**, 110812 (2022).
15. K. H. D. Crawford *et al.*, Protocol and Reagents for Pseudotyping Lentiviral Particles with SARS-CoV-2 Spike Protein for Neutralization Assays. *Viruses* **12** (2020).
16. A. G. Farrell *et al.*, Receptor-Binding Domain (RBD) Antibodies Contribute More to SARS-CoV-2 Neutralization When Target Cells Express High Levels of ACE2. *Viruses* **14** (2022).
17. T. N. Starr *et al.*, Deep Mutational Scanning of SARS-CoV-2 Receptor Binding Domain Reveals Constraints on Folding and ACE2 Binding. *Cell* **182**, 1295-1310 e1220 (2020).
18. T. N. Starr *et al.*, Deep mutational scans for ACE2 binding, RBD expression, and antibody escape in the SARS-CoV-2 Omicron BA.1 and BA.2 receptor-binding domains. *PLoS Pathog* **18**, e1010951 (2022).
19. B. Dadonaite *et al.*, A pseudovirus system enables deep mutational scanning of the full SARS-CoV-2 spike. *Cell* **186**, 1263-1278 e1220 (2023).
20. K. Katoh, J. Rozewicki, K. D. Yamada, MAFFT online service: multiple sequence alignment, interactive sequence choice and visualization. *Brief Bioinform* **20**, 1160-1166 (2019).
21. A. M. Waterhouse, J. B. Procter, D. M. Martin, M. Clamp, G. J. Barton, Jalview Version 2--a multiple sequence alignment editor and analysis workbench. *Bioinformatics* **25**, 1189-1191 (2009).
22. C. L. Hsieh *et al.*, Structure-based design of prefusion-stabilized SARS-CoV-2 spikes. *Science (New York, N.Y.)* **369**, 1501-1505 (2020).
23. T. Wagner *et al.*, SPHIRE-crYOLO is a fast and accurate fully automated particle picker for cryo-EM. *Commun Biol* **2**, 218 (2019).

24. D. Kimanius, L. Dong, G. Sharov, T. Nakane, S. H. W. Scheres, New tools for automated cryo-EM single-particle analysis in RELION-4.0. *Biochem J* **478**, 4169-4185 (2021).
25. A. Kucukelbir, F. J. Sigworth, H. D. Tagare, Quantifying the local resolution of cryo-EM density maps. *Nature methods* **11**, 63-65 (2014).
26. E. F. Pettersen *et al.*, UCSF Chimera--a visualization system for exploratory research and analysis. *J Comput Chem* **25**, 1605-1612 (2004).
27. E. F. Pettersen *et al.*, UCSF ChimeraX: Structure visualization for researchers, educators, and developers. *Protein Sci* **30**, 70-82 (2021).